Accelerated Publications

Structural Characterization of the Stringent Response Related Exopolyphosphatase/Guanosine Pentaphosphate Phosphohydrolase Protein Family[†,‡]

Ole Kristensen,*[,§] Martin Laurberg,[⊥,||] Anders Liljas,[⊥] Jette Sandholm Kastrup,[§] and Michael Gajhede[§]

Biostructural Research, Department of Medicinal Chemistry, The Danish University of Pharmaceutical Sciences, Universitetsparken 2, DK-2100 Copenhagen, Denmark, and Molecular Biophysics, Lund University, Getingevägen 60, SE-221 00 Lund, Sweden

Received May 6, 2004; Revised Manuscript Received May 30, 2004

ABSTRACT: Exopolyphosphatase/guanosine pentaphosphate phosphohydrolase (PPX/GPPA) enzymes play central roles in the bacterial stringent response induced by starvation. The high-resolution crystal structure of the putative *Aquifex aeolicus* PPX/GPPA phosphatase from the actin-like ATPase domain superfamily has been determined, providing the first insights to features of the common catalytic core of the PPX/GPPA family. The protein has a two-domain structure with an active site located in the interdomain cleft. Two crystal forms were investigated (type I and II) at resolutions of 1.53 and 2.15 Å, respectively. This revealed a structural flexibility that has previously been described as a "butterfly-like" cleft opening around the active site in other actin-like superfamily proteins. A calcium ion is observed at the center of this region in type I crystals, substantiating that PPX/GPPA enzymes use metal ions for catalysis. Structural analysis suggests that nucleotides bind at a similar position to that seen in other members of the superfamily.

Bacteria have developed systems that allow them to adjust to sudden changes in the environment. The mechanisms that operate in the global regulation of cellular metabolism when the supply of essential nutrients such as amino acids, carbon, and phosphate are abruptly deprived are referred to as the stringent response (*1*). The stringent response initiated upon amino acid starvation has been extensively studied in *Eschericia coli*, including the accumulation of inorganic polyphosphate (polyP)[1] and guanosine tetraphosphate (ppGpp). The intricate system that is activated under such circumstances coordinates changes in protein synthesis, transcription, and protein degradation (*2*−*4*).

Nutritional downshift results in an increased number of uncharged transfer RNA molecules reaching the ribosome. This activates the ribosome-bound protein stringent factor (SF or RelA) (*5*, *6*). Once activated, SF catalyzes a pyrophosphoryl transfer from ATP to the 3′-hydroxyl group of GTP forming guanosine pentaphosphate, pppGpp (*7*, *8*). SF can also accept GDP as a substrate for synthesizing ppGpp. However, recent data imply that GTP and not GDP associates with SF under stringent response conditions (*6*).

The *E. coli* gppA gene product (GPPA) regulates the conversion of pppGpp to the biologically effective second messenger ppGpp, known as the "magic spot I" (*9*, *10*). Increased levels of ppGpp are known to affect the level of exopolyphosphatase (PPX) activity in many species. In *E. coli*, the GPPA and PPX enzymes share extensive sequence identity. A consequence of reduced PPX activity is a dramatic shift in the equilibrium between polyP breakdown and accumulation catalyzed by polynucleotide kinase, PPK (*3*, *4*). Subsequently, association of polyP with the Lon protease controls degradation of free ribosomal protein as observed in bacteria during starvation. Thus, both GPPA and PPX play central roles in this regulatory system.

The *Aquifex aeolicus* genome has been fully sequenced, and a single 35.5 kDa protein represents the PPX/GPPA family in this organism (*11*). The encoding gene has been annotated as an exopolyphosphatase, *ppx*. However, this extremophile lacks PPK-coding genes (*12*), which suggests that the primary function of the *A. aeolicus* PPX/GPPA protein is to provide GPPA activity.

Here, we present the structure of the *A. aeolicus* PPX/GPPA enzyme based on X-ray diffraction experiments. This structure provides the first insights into structure/function relationships of the PPX/GPPA family.

[†] This work was supported by grants from DANSYNC (www.dansync.dk) and the Swedish Research Council (Grant 03262-344).

[‡] Coordinates for the type I and type II structures have been deposited with the Protein Data Bank as entries 1T6C and 1T6D, respectively.

* To whom correspondence should be addressed. E-mail: ok@dfuni.dk. Phone: +45 3530 6121. Fax: +45 3530 6040.

[§] The Danish University of Pharmaceutical Sciences.

[⊥] Lund University.

[||] Present address: Center for Molecular Biology of RNA, Sinsheimer Laboratories, University of California at Santa Cruz, CA 95064.

[1] Abbreviations: GPPA, gppA gene product; NCS, noncrystallographic symmetry; polyP, inorganic polyphosphate; ppGpp, guanosine tetraphosphate; PPK, polynucleotide kinase; pppGpp, guanosine pentaphosphate; PPX, exopolyphosphatase; PPX/GPPA, exopolyphosphatase/guanosine pentaphosphate phosphohydrolase; SF, ribosome-bound protein stringent factor; MES, 2-(*N*-morpholine)ethanesulfonic acid; MPD, methylpentanediol; PEG, poly(ethylene glycol); SAD, single-wavelength anomalous diffraction; rmsd, root mean square deviation; Hsc70, bovine heat shock 70 protein; DTT, dithiothreitol.

10.1021/bi049083c CCC: $27.50
Published on Web 06/19/2004

Table 1: Summary of Data Collection, Phase Determination, and Refinement

	type I, native	type II, SeMet	type II, SeMet-$YbCl_2$
Data Collection			
X-ray source	BL711/MaxLab	ID14.1/ESRF	BL711/MaxLab
resolution range (Å)	15−1.53 (1.61−1.53)[a]	30−2.15 (2.27−2.15)	20−2.25 (2.37−2.25)
unique reflections	47 505 (5936)	66 436 (10 090)	56 064 (7781)
average multiplicity	6.9 (2.7)	5.5 (5.5)	2.3 (2.2)
completeness, %	95.8 (84.6)	99.9 (100.0)	94.6 (88.8)
$\langle I/(\sigma I)\rangle$	22.8 (2.2)	23.3 (8.8)	24.9 (3.7)
R_{merge},[b] %	6.9 (34.1)	7.6 (28.7)	6.9 (36.0)
Phasing			
heavy atom sites		6Se	6Se, 4Yb
resolution range (Å)		30−2.15	20−2.25
figure of merit (acentric/centric)		0.35/0.17	
phasing power (iso/ano)[c]		−/0.68	0.84/0.96
R_{cullis} (iso/ano)[d]		−/0.92	0.88/0.86
Refinement			
R_{work}/R_{free}[e] (%)	16.2/21.7	20.6/25.5	
number of atoms			
protein	2528	4852	
water	390	340	
hetero	53	10	
average *B*-factor (Å^2)			
protein	18	35	
water	33	40	
$Cl^-/I^-/Ca^{2+}$/MPD/Tris	22/15/14/42/−	24/−/−/−/58	
rms deviation			
bond lengths (Å)	0.013	0.005	
angles (deg)	1.5	1.1	
Ramachandran plots (*64*) (% residues, favored/allowed)	96.3/100.0	93.3/99.5	

[a] Values in parentheses refer to the highest resolution bin (e.g., 1.61−1.53 Å). [b] $R_{merge} = \sum_{hkl}(\sum_i(|I_{hkl,i} - \langle I_{hkl}\rangle|))/\sum_{hkl,i}\langle I_{hkl}\rangle$, where $I_{hkl,i}$ is the intensity of an individual measurement of the reflection with Miller indicies *h*, *k*, and *l*, and $\langle I_{hkl}\rangle$ is the mean intensity of that reflection. [c] Phasing power $= \sum_{hkl}F_{H,hkl}/\sum_{hkl}|F_{PH,obsd,hkl} - F_{PH,calcd,hkl}|$. [d] $R_{cullis} = \sum_{hkl}||F_{PH,hkl} \pm F_{P,hkl}| - F_{H,calcd,hkl}|/\sum_{hkl}|F_{PH,hkl} - F_{P,hkl}|$, where F_{PH} is the structure factor of the heavy atom derivative, F_P is the structure factor of the native protein, and $F_{H,calcd}$ is the calculated structure factor for the heavy atom. [e] $R_{work} = \sum_{hkl}(||F_{obsd,hkl}| - |F_{calcd,hkl}||)/|F_{obsd,hkl}|$, where $|F_{obsd,hkl}|$ and $|F_{calcd,hkl}|$ are the observed and calculated structure factor amplitudes. R_{free} is equivalent to the R_{work} but calculated with 1% (type I) and 2% (type II) of the reflections omitted from the refinement process.

EXPERIMENTAL PROCEDURES

Preparation of PPX/GPPA Enzyme. The details for expression, mutagenesis, purification, and crystallization of the *A. aeolicus* PPX/GPPA enzyme have been described previously (*13*). In summary, the gene was amplified by PCR from genomic DNA (*11*) and cloned as an N-terminal His-tagged construct in the vector pET28a (Novagen). A triple mutant version of the construct (V82M, C138M, and V306M) was prepared using PCR primers and repeated restriction enzyme digestions. The triple mutant protein was expressed as a selenomethionine variant according to a published procedure (*14*). All proteins used in this study were purified on metal-affinity resins followed by thrombin cleavage of the His-tag and Superdex 200 (Pharmacia) gel filtration. A calcium-ion containing thrombin cleavage buffer was used in preparation of the sample for the type I crystals. However, the final gel filtration buffer was not supplemented with any calcium salts. For the preparation of type II crystals, calcium ions were not introduced during the purification.

Crystallization: Type I Crystals. Plate-shaped crystals of native PPX/GPPA were produced by the vapor diffusion hanging drop method in a solution containing 57% methylpentanediol (MPD), 0.1 M 2-(*N*-morpholino)ethanesulfonic acid (MES), 0.05−0.07 M Tris-base, 0.14 M KCl, 0.005 M dithiothreitol (DTT), providing a pH in the range 6.2−6.6. The crystals of this form belong to the orthorhombic space group $P2_12_12_1$ with unit cell parameters $a = 50.8$, $b = 70.3$, and $c = 90.8$ Å and contain one molecule per asymmetric unit. The crystals diffracted to a maximum resolution of 1.53 Å. These crystals were soaked in a solution containing K_2HgI_4 with an excess of KI and later used for refinement. Except for the putative iodide ion, no Hg^{2+} ions were observed in the crystal structure. Other lower resolution structures have been determined (data not shown) from crystals that had not been soaked with heavy atom compounds. Comparison of these structures to the structure from the soaked crystals revealed no significant differences; hence, it is reasonable to denote it as a native crystal (Table 1).

Crystallization: Type II Crystals. Different conditions were identified to crystallize deliberately oxidized selenomethionine triple-mutant protein: 26% poly(ethylene glycol) (PEG) 4000, 5% PEG 400, 0.1 M Tris-base, 0.06−0.02 M acetic acid, 0.15 M $MgCl_2$, pH 8−8.5. The protein sample was purified in the absence of reducing agents and incubated with 0.1% H_2O_2 prior to crystallization. Monoclinic $P2_1$ crystals obtained under these conditions diffracted to 2.15 Å, have cell dimensions of $a = 54.5$ Å, $b = 83.5$ Å, $c = 69.8$ Å, and $\beta = 97.4°$, and contained two molecules per asymmetric unit. An isomorphous ytterbium derivative was prepared by addition of $YbCl_3$ directly to a type II crystallization droplet at a concentration of approximately 0.5 M.

Structure Determination. Experimental phases were derived from X-ray data collected on type II crystals, including single-wavelength anomalous diffraction (SAD) selenom-

ethionine data and anomalous data obtained from an ytterbium derivative collected at wavelengths of 0.934 and 0.970 Å, respectively (Table 1). X-ray data sets were processed using the CCP4 program suite (*15*). The heavy atom substructures were initially analyzed with the program SOLVE (*16*), and the identified heavy atom sites were subsequently used to optimize the derived phases using SHARP (*17*). A partial model was produced using the program Arp/Warp (*18*), comprising 145 out of 315 residues. This model was used for molecular replacement in the program CNS (*19*) with the high-resolution type I data. The Arp/Warp procedure was applied again using these data. Rapid convergence with 283 residues traced in 100 cycles resulted in a nearly complete model. On this basis, it was straightforward to complete the type II structure determination by molecular replacement.

The type I and type II structures were refined by REFMAC5 and CNS, respectively (*19*, *20*). Modest NCS restraints were applied in the early stage of the type II refinement. Data collection, phasing, and refinement statistics are summarized in Table 1. The programs Molscript, Raster3D, Alscript, Ribbons, and Pymol were used in the preparation of figures (*21*−*25*). Model phases were derived from the refined type I structure excluding all calcium, chloride, and iodide ions and used to calculate an anomalous difference electron density map, see Figure 3A,B.

RESULTS

Overall Structure. The type I structure of *A. aeolicus* PPX/GPPA is shown in cartoon representation in Figure 1A. The structure is comprised of two domains, each with a fold that contains the ribonuclease H-like motif, as predicted by Bork, Sander, and co-workers (*26*). The connecting helix 2 involved in domain separation (*26*, *27*) was however erroneously predicted, see Figure 2.

This architecture characterizes the actin-like ATPase domain superfamily. The ribonuclease H-like motif consists of a mixed five-stranded β-sheet with the second strand antiparallel to the rest. The connections between strand 1 and strand 4 and between strand 4 and strand 5 contain helical segments, all on the same side of the sheet. The connections are significantly longer in the C-terminal domain than in the N-terminal domain. Accordingly, five α-helices are present in the C-terminal domain and only two in the N-terminal domain. The two domains can be aligned with an rmsd of 1.9 Å using 47 Cα-atoms. In both domains, the other side of the sheet is flanked by the N-terminal helix of the other domain.

The type I crystal structure represents a somewhat closed domain configuration. One of the two PPX/GPPA molecules (molecule A) of the type II structure is similar to the type I structure, whereas the second molecule (molecule B) displays a more open arrangement of the domains. The rotational movement of the two domains around a single hinge region (residues 122−123) is 11.5° in molecule B and almost insignificant in molecule A relative to the type I structure. The type I and the type II (molecule B) configurations are superimposed in Figure 1B. This reveals a structural flexibility that has previously been described as a "butterfly-like" cleft opening around the active site in other actin-like superfamily proteins (*28*).

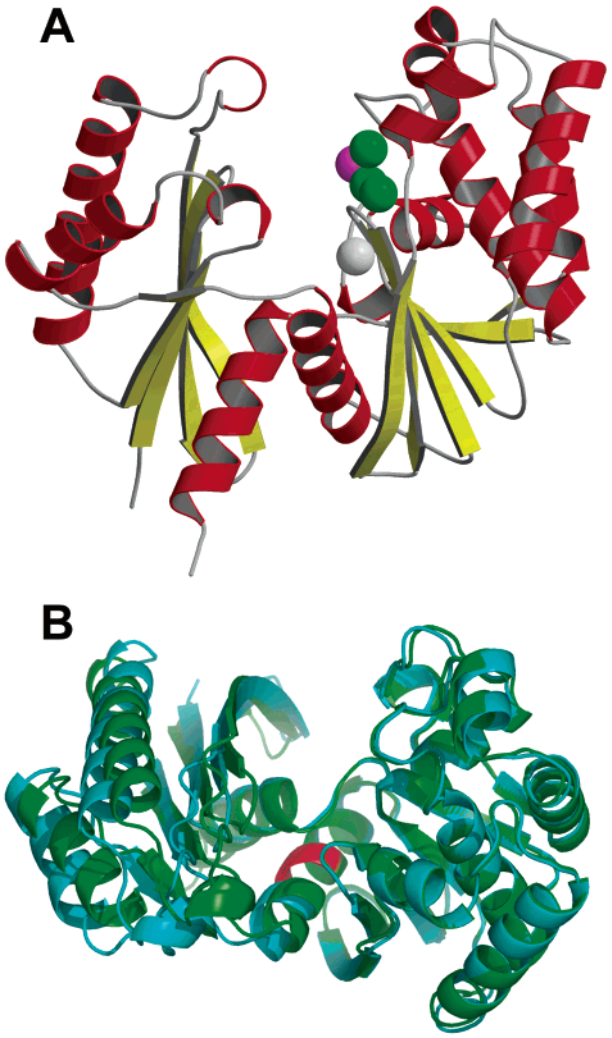

FIGURE 1: Outline of the common structural core of the PPX/GPPA protein family. Panel A shows a cartoon of the type I structure. The overall fold of PPX/GPPA enzymes shows a clear similarity to other proteins of the actin-like ATPase domain superfamily. The N-terminal domain (to the left) is separated from the C-terminal domain (to the right) by two α-helices at the center of the structure. Three chloride ions (green spheres) and a calcium ion (grey sphere) indicate the position of the active site. A putative iodide ion with no anticipated functional significance is shown in magenta. Panel B shows the superimposition of the type I and II structures. The type II structure (cyan, molecule B) was structurally aligned with the type I structure (green) using the C-terminal domain as a common reference. The structural flexibility displayed in this representation was analyzed by the program DYNDOM (*65*). A single hinge region accounting for rotational flexibility of the domain configuration (11.5°) was unambiguously identified around residues 122−123 (colored red).

Ion Binding Sites. A Ca^{2+} binding site is observed close to the short loop between strands 2 and 3 of the C-terminal domain in the native type I crystal structure, see Figure 3A. The ion is heptacoordinated, and it is ligated by two water molecules, three backbone carbonyls (residues 141, 143, and 146), and side chain oxygens of Glu148 and Ser146. The conformation and side chain positions of this loop are similar in the non-calcium-containing type II crystals, but differences in the water structure are observed. Difference electron density maps show the absence of a highly occupied metal-ion-binding site in the type II structure, and a water molecule was modeled at this position.

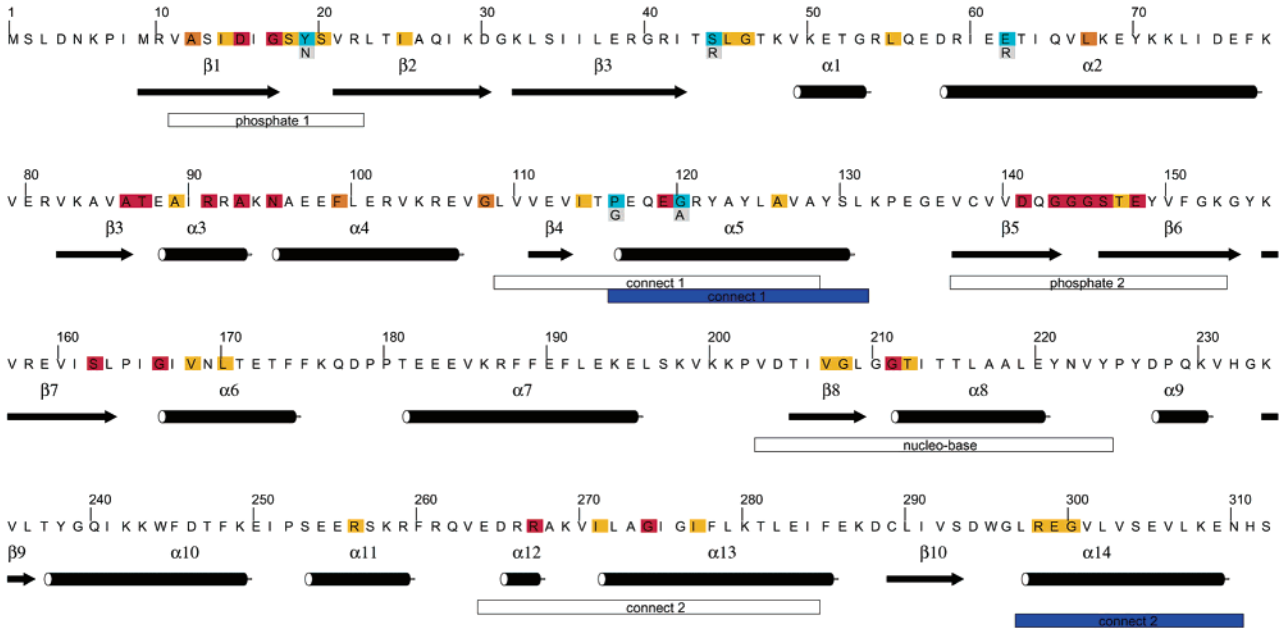

FIGURE 2: Conservation of sequence and structural elements within the family of PPX/GPPA phosphatases. The sequence of the *A. aeolicus* PPX/GPPA enzyme is flanked by schematic symbols (black) that mirror the secondary structure of our crystal structures. Below these, open rectangles show the positions of the structural signatures identified by Bork, Sander, and co-workers (*26*). Blue rectangles indicate the correct positions of the domain separating helices (connect 1 and connect 2). Twenty of the most similar PPX/GPPA sequences were aligned by CLUSTALW (*66*). Residues boxed with red color are fully conserved in all 20 sequences, orange color indicates conservation in 19 out of 20 sequences, and yellow boxes show other residues that are highly conserved. Residues marked with cyan color are also highly conserved within the family, but the sequence of the extremophile *A. aeolicus* has unusual residues at these positions. The identity of the most dominant amino acids at these positions is shown in gray boxes.

Three chloride ions and one iodide ion are found in the type I PPX/GPPA structure, see Figure 3B. The iodide ion is located in a nonpolar pocket around residues Tyr224, Pro225, and Tyr226. One of the chloride ions is present in all molecules of the type I and type II structures. Main-chain amides (closest contacts Gly145 and Ile167) and the side chain of Gln142 (NE2) exclusively provide the anion interactions. The other two chloride ions are only present in the type I structure with closest contacts to Gln142 (NE2) and Asn169(N), respectively.

DISCUSSION

The *A. aeolicus* PPX/GPPA structure is the first representative of the Pfam PPX/GPPA family that currently comprises 124 members (*29*). Neither the location of the active site nor the catalytic mechanism for this family has previously been reported. However, conservation of amino acid residues can provide information on the location of the active site. Figure 4 shows a cartoon representation of PPX/GPPA colored after sequence entropy, based on comparison with the 20 most similar sequences from a BLAST search (*30*). This comparison strongly suggests that the active site is located in the cleft between the two domains, an active site position also found in the structurally related enzymes in the actin-like ATPase domain superfamily.

The structure of PPX/GPPA is most similar to the hydroxyglutaryl-CoA dehydratase component A family within the actin-like ATPase domain superfamily according to a search using the DALI server (*31*). In addition, the structure is closely related to the acetate kinase and hexokinase families. Sequence identities are in the range 7−15%, and the rms deviations including about 200 Cα-atoms are around 4 Å. The superfamily of actin-like ATPase domains comprises a total of six families: actin/HSP70, hydroxyglutaryl-CoA dehydratase component A, acetate kinase, ATPase domain of the glycerol dehydratase reactivase α subunit, hexokinase, and glycerol kinase (*32*). Within this superfamily, a total of 17 structures of enzyme−nucleotide/nucleotide analogue complexes have been determined (*33*−*48*). Within the superfamily of actin-like ATPase domain enzymes, domain movements up to 30° are observed to be involved in catalysis (*49*). In the type I and type II structures of *A. aeolicus* PPX/GPPA, a similar flexibility is seen. Because only a relatively small variation in domain rotation (up to 11.5°) is observed among the three molecules, even larger movements can be envisioned.

The locations of the nucleotides from representative structures superimposed on the PPX/GPPA enzyme using the program Top (*50*) are shown in Figure 4. The nucleotides are located at similar positions. The nucleobases stack at an often-helical segment following immediately after *β*-strand 4 of the C-terminal domain. This helix is also found in PPX/GPPA, and it is possible that the potential guanosine base also binds here. It would however require a significantly different hinge angle. It is important to note that base specificity is not a general key issue. The 3′-pyrophosphate provides an additional substrate tag, and at least in the most well studied organism, *E. coli*, hyperphosphorylated adenine nucleotides do not appear to accumulate under stringent response (*51*).

In other structures of the actin-like ATPase domain enzymes, phosphates bind between the two hairpin loops connecting *β*-strands 2 and 3 in each of the ribonuclease H-like motifs. The N-terminal loop of *A. aeolicus* PPX/GPPA contains a highly conserved DXGS[Y/N]S motif, which to date has not been included in the Pfam signature (*29*). The

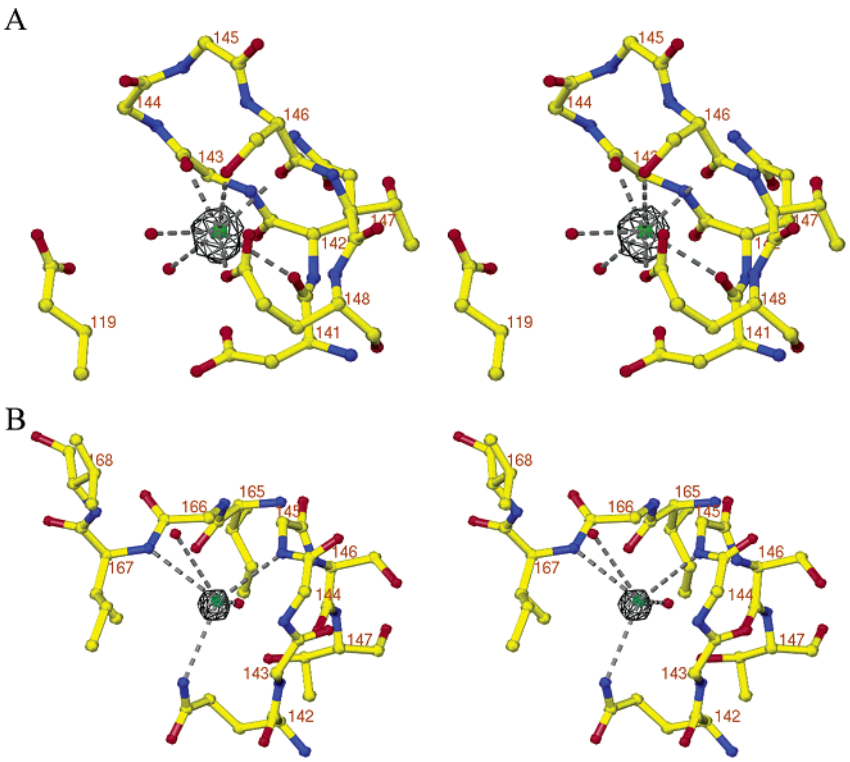

FIGURE 3: Calcium ion and chloride ion binding sites in the PPX/GPPA type I structure. Panel A presents the calcium site. The C-terminal PPX/GPP domain harbors a variant of the Walker B motif in a highly conserved loop region. Both side-chain atoms and backbone carbonyl oxygens participate in direct binding of the metal ion. This heptacoordinated calcium ion is bound at the center of the active site in agreement with the established requirement for divalent metal ions in PPX/GPPA catalysis. Distances from the calcium ion to the coordinating backbone carbonyl atoms of residues 141, 143, and 146 are 2.87, 2.63, and 2.74 Å, respectively. The two bound water molecules are located 2.75 and 2.77 Å from the calcium ion, and the side chain oxygens of Glu148 and Ser146 have coordination distances of 2.68 and 3.23 Å. The displayed (4.0σ threshold) anomalous difference electron map (see Experimental Procedures) sustains the assignment of the ion as calcium. The conserved Glu119 is located in this region, and it has most likely an important functional role. Panel B presents the chloride site. One chloride ion is consistently observed in both molecules of the type II structure and in the type I structure at a position opposite to the calcium ion. It is possible that this feature mirrors the position of a structural oxy-anion pocket formed to accommodate substrate binding. Distances to the nearest nitrogen atoms are 3.26 (Gln142-NE2), 3.29 (Gly145-N), and 3.35 Å (Ile167-N). Assignment of this chloride ion is supported by the anomalous difference electron density map shown in black color (4.0σ threshold).

C-terminal loop of PPX/GPPA harbors a conserved variant of the Walker B (*52*) motif [D/E]-X-G-G-[G/A]-S-X-E, corresponding to residues 141−148 in *A. aeolicus*. Other members of the actin-like ATPase domain superfamily also contain a Walker B related motif or phosphate 2 loop (*26*). In conclusion, it is likely that the potential substrate, pppGpp, would also bind at a similar location as that seen in other actin-like ATPase domain complexes, in agreement with the suggestions of Bork, Sander, and co-workers (*26*).

Structural studies of these enzymes show that the first residue (usually an aspartate) of the Walker B motif participates in water-mediated magnesium binding (*33*−*48*). However, in *A. aeolicus* PPX/GPPA, we find that the C-terminal Glu148 of the motif participates directly in binding to a Ca^{2+} ion. The conserved nature of the metal ion coordinating residues and the suggested strong affinity indicate that PPX/GPPA phosphatase catalyzed reactions may depend on calcium ions. However, requirements for Mg^{2+} in millimolar concentrations have previously been reported for PPX/GPPA enzymes (*53*, *54*). In both of the molecules of the type II crystal structure, metal ions could not be modeled with confidence at this position despite that the crystal was obtained from a solution containing 150 mM $MgCl_2$. A preloaded calcium ion would neutralize the acidic environment around the residues Glu148 and Asp141 of PPX/GPPA and allow the highly negatively charged 5′-phosphate tail to enter the active site. Calcium ions have high variability in coordination geometry (*55*), which has been suggested as an advantage (*56*).

Chloride ions from the crystallization medium have previously been found to mirror functional characteristics of, for example, active site carboxylate and phosphate groups (*57*). Three chloride ions are likewise found close to the active site of PPX/GPPA in the type I crystal. We suggest that at least the chloride ion present also in both molecules of the type II structure may structurally mirror the location of a substrate 3′-phosphate.

Activation of a nucleophile in the substrate-binding site has been implied as an important factor both in members of the actin-like ATPase superfamily and other nucleotidases (*28*, *41*). Site-directed mutagenesis has been used to study the mechanism of hydrolysis in several members of the actin-like ATPase superfamily (*28*). While this approach has proven useful to dissect the mechanism of NTP hydrolysis by some P-loop proteins, the nucleotide-binding site of actin-fold proteins is often distorted by mutations (*28*, *58*−*61*). Usually, either hydroxyl ions or water molecules have been suggested as the nucleophiles acting in hydrolysis. Carboxylate groups of side chains involved in the binding of divalent metal ions in the bovine heat-shock 70 (Hsc70) protein (Glu175), hexokinase (Asp211), and glycerol kinase (Asp245) structures have been identified as the catalytic bases respon-

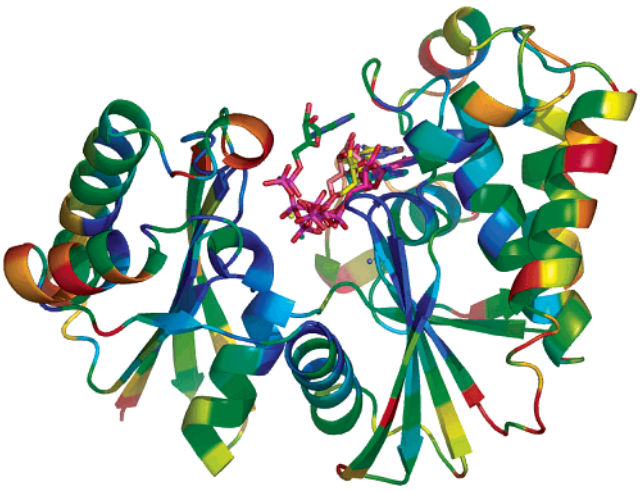

FIGURE 4: Superpositions of actin-like ATPase domain superfamily members and sequence entropy within the PPX/GPPA protein family. The PPX/GPPA structure is shown as a cartoon with color ramping according to the sequence entropy, as implemented in the program Indonesia (http://xray.bmc.uu.se/dennis). A blue color represents highly conserved regions. Seventeen examples of protein/ligand complexes in the actin-like ATPase domain superfamily have been compiled in this figure, revealing a remarkable similarity in the positions of the ligands in the active site region.

sible for nucleophile generation (*28*). However, mutational analyses have shown that also other carboxylic side chains are required to achieve full catalytic activity (*28*). Consequently, we suggest that the PPX/GPPA family of proteins use metal coordination and the strictly conserved residues Asp141 and Glu148 (see Figure 2) as the basis for a catalytic environment. The conserved residue Glu119 is within 5 Å of the metal binding site, and it is likely that it also has a role in catalysis, possibly providing an active site base.

A hydroxyl ion coordinated by Lys71 in the heat-shock 70 proteins has been suggested as the likely active site nucleophile, while the structurally equivalent Arg177 residue in actin is not required for catalysis (*28*, *60*). In the *A. aeolicus* PPX/GPPA structures, the basic residues of the conserved and domain-duplicated RRAK motif (residues 91−94 and 266−269) are found at positions corresponding approximately to the Lys71 in the heat-shock 70 proteins. However, the rare left-handed $\beta\alpha\beta$-crossover configuration of the RRAK motif is only preserved in the N-terminal domain. This unusual $\beta\alpha\beta$-motif has previously been suggested as a conserved feature in a superfamily of nucleic acid binding domains and the positive charge of the loop region to be implicated in phosphate binding (*62*, *63*). Yet, even in the most closed conformation, we observe that the basic residues in the N-terminal RRAK motif of the PPX/GPPA structure are too far from the anticipated active site around the calcium binding position.

In conclusion, the structure of *A. aeolicus* PPX/GPPA provides the first insights into the catalytic mechanisms of this family of enzymes. Detailed structural information on binding of nucleotides will await cocrystallization of such complexes.

ACKNOWLEDGMENT

We appreciate the persistent support in data collection from the staff at the MaxLab, BL711, and ESRF, ID14.1.

REFERENCES

1. Balzer, G. J., and McLean, R. J. (2002) The stringent response genes relA and spoT are important for *Escherichia coli* biofilms under slow-growth conditions, *Can. J. Microbiol. 48*, 675−680.
2. Artsimovitch, I., Patlan, V., Sekine, S., Vassylyeva, M. N., Hosaka, T., Ochi, K., Yokoyama, S., and Vassylyev, D. G. (2004) Structural basis for transcription regulation by alarmone ppGpp, *Cell 117*, 299−310.
3. Gottesman, S., and Maurizi, M. R. (2001) Cell biology. Surviving starvation, *Science 293*, 614−615.
4. Kuroda, A., Nomura, K., Ohtomo, R., Kato, J., Ikeda, T., Takiguchi, N., Ohtake, H., and Kornberg, A. (2001) Role of inorganic polyphosphate in promoting ribosomal protein degradation by the Lon protease in *E. coli*, *Science 293*, 705−708.
5. Ogawa, Y., and Sy, J. (1977) Synthesis of guanosine polyphosphates (pppGpp and ppGpp) and its regulation by aminoacyl-tRNA, *J. Biochem. (Tokyo) 82*, 947−953.
6. Wendrich, T. M., Blaha, G., Wilson, D. N., Marahiel, M. A., and Nierhaus, K. H. (2002) Dissection of the mechanism for the stringent factor RelA, *Mol. Cell 10*, 779−788.
7. Hogg, T., Mechold, U., Malke, H., Cashel, M., and Hilgenfeld, R. (2004) Conformational antagonism between opposing active sites in a bifunctional RelA/SpoT homologue modulates (p)ppGpp metabolism during the stringent response, *Cell 117*, 57−68.
8. Gropp, M., Strausz, Y., Gross, M., and Glaser, G. (2001) Regulation of *Escherichia coli* RelA requires oligomerization of the C-terminal domain, *J. Bacteriol. 183*, 570−579.
9. Keasling, J. D., Bertsch, L., and Kornberg, A. (1993) Guanosine pentaphosphate phosphohydrolase of *Escherichia coli* is a long-chain exopolyphosphatase, *Proc. Natl. Acad. Sci. U.S.A. 90*, 7029−7033.
10. Kuroda, A., Murphy, H., Cashel, M., and Kornberg, A. (1997) Guanosine tetra- and pentaphosphate promote accumulation of inorganic polyphosphate in *Escherichia coli*, *J. Biol. Chem. 272*, 21240−21243.
11. Deckert, G., Warren, P. V., Gaasterland, T., Young, W. G., Lenox, A. L., Graham, D. E., Overbeek, R., Snead, M. A., Keller, M., Aujay, M., Huber, R., Feldman, R. A., Short, J. M., Olsen, G. J., and Swanson, R. V. (1998) The complete genome of the hyperthermophilic bacterium *Aquifex aeolicus*, *Nature 392*, 353−358.
12. Zhang, H., Ishige, K., and Kornberg, A. (2002) A polyphosphate kinase (PPK2) widely conserved in bacteria, *Proc. Natl. Acad. Sci. U.S.A. 99*, 16678−16683.
13. Kristensen, O., Laurberg, M., and Gajhede, M. (2002) Crystallization of a stringent response factor from *Aquifex aeolicus*, *Acta Crystallogr., Sect. D: Biol. Crystallogr. 58*, 1198−1200.
14. Van Duyne, G. D., Standaert, R. F., Karplus, P. A., Schreiber, S. L., and Clardy, J. (1993) Atomic structures of the human immunophilin FKBP-12 complexes with FK506 and rapamycin, *J. Mol. Biol. 229*, 105−124.
15. Collaborative Computational Project No. 4 (1994) The CCP4 suite: Programs for protein crystallography, *Acta Crystallogr., Sect. D: Biol. Crystallogr. 50*, 760−763.
16. Terwilliger, T. C., and Berendzen, J. (1999) Automated MAD and MIR structure solution, *Acta Crystallogr., Sect. D: Biol. Crystallogr. 55* (Pt 4), 849−861.
17. Fortelle, E. D. L., and Bricogne, G. (1997) Maximum-likelihood heavy-atom parameter refinement for multiple isomorphous replacement and multiwavelength anomalous diffraction methods, *Methods Enzymol. Macromol. Crystallogr. Part A 276*, 472−494.
18. Lamzin, V. S., Perrakis, A., and Wilson, K. S. (2001) The ARP/wARP suite for automated construction and refinement of protein models, *Int. Tables Crystallogr. F*, 720−722.
19. Brunger, A. T., Adams, P. D., Clore, G. M., DeLano, W. L., Gros, P., Grosse-Kunstleve, R. W., Jiang, J. S., Kuszewski, J., Nilges, M., Pannu, N. S., Read, R. J., Rice, L. M., Simonson, T., and Warren, G. L. (1998) Crystallography & NMR system: A new software suite for macromolecular structure determination, *Acta Crystallogr., Sect. D: Biol. Crystallogr. 54* (Pt 5), 905−921.
20. Pannu, N. S., Murshudov, G. N., Dodson, E. J., and Read, R. J. (1998) Incorporation of prior phase information strengthens maximum-likelihood structure refinement, *Acta Crystallogr., Sect. D: Biol. Crystallogr. 54*, 1285−1294.
21. Kraulis, P. J. (1991) MOLSCRIPT: A program to produce both detailed and schematic plots of protein structures, *J. Appl. Crystallogr. 24*, 946−950.

22. Merritt, E. A., and Bacon, D. J. (1997) Raster3D: Photorealistic molecular graphics, *Methods Enzymol. 277*, 505−524.
23. Barton, G. J. (1993) ALSCRIPT: A tool to format multiple sequence alignments, *Protein Eng. 6*, 37−40.
24. Carson, M. (1997) Ribbons, *Methods Enzymol. 277*, 493−505.
25. DeLano, W. L. (2002) *PyMol*, DeLano Scientific, San Carlos, CA.
26. Reizer, J., Reizer, A., Saier, M. H., Jr., Bork, P., and Sander, C. (1993) Exopolyphosphate phosphatase and guanosine pentaphosphate phosphatase belong to the sugar kinase/actin/hsp 70 superfamily, *Trends Biochem. Sci. 18*, 247−248.
27. Cardona, S. T., Chavez, F. P., and Jerez, C. A. (2002) The exopolyphosphatase gene from *Sulfolobus solfataricus*: Characterization of the first gene found to be involved in polyphosphate metabolism in Archaea, *Appl. Environ. Microbiol. 68*, 4812−4819.
28. Schuler, H. (2001) ATPase activity and conformational changes in the regulation of actin, *Biochim. Biophys. Acta 1549*, 137−147.
29. Bateman, A., Coin, L., Durbin, R., Finn, R. D., Hollich, V., Griffiths-Jones, S., Khanna, A., Marshall, M., Moxon, S., Sonnhammer, E. L., Studholme, D. J., Yeats, C., and Eddy, S. R. (2004) The Pfam protein families database, *Nucleic Acids Res. 32*, D138−D141 (database issue).
30. Altschul, S. F., and Lipman, D. J. (1990) Protein database searches for multiple alignments, *Proc. Natl. Acad. Sci. U.S.A. 87*, 5509−5513.
31. Holm, L., and Sander, C. (1993) Protein structure comparison by alignment of distance matrices, *J. Mol. Biol. 233*, 123−138.
32. Murzin, A. G., Brenner, S. E., Hubbard, T., and Chothia, C. (1995) SCOP: A structural classification of proteins database for the investigation of sequences and structures, *J. Mol. Biol. 247*, 536−540.
33. Vorobiev, S., Strokopytov, B., Drubin, D. G., Frieden, C., Ono, S., Condeelis, J., Rubenstein, P. A., and Almo, S. C. (2003) The structure of nonvertebrate actin: Implications for the ATP hydrolytic mechanism, *Proc. Natl. Acad. Sci. U.S.A. 100*, 5760−5765.
34. Chik, J. K., Lindberg, U., and Schutt, C. E. (1996) The structure of an open state of beta-actin at 2.65 Å resolution, *J. Mol. Biol. 263*, 607−623.
35. Dawson, J. F., Sablin, E. P., Spudich, J. A., and Fletterick, R. J. (2003) Structure of an F-actin trimer disrupted by gelsolin and implications for the mechanism of severing, *J. Biol. Chem. 278*, 1229−1238.
36. Graceffa, P., and Dominguez, R. (2003) Crystal structure of monomeric actin in the ATP state. Structural basis of nucleotide-dependent actin dynamics, *J. Biol. Chem. 278*, 34172−34180.
37. van den Ent, F., and Lowe, J. (2000) Crystal structure of the cell division protein FtsA from *Thermotoga maritima*, *EMBO J. 19*, 5300−5307.
38. van den Ent, F., Amos, L. A., and Lowe, J. (2001) Prokaryotic origin of the actin cytoskeleton, *Nature 413*, 39−44.
39. van den Ent, F., Moller-Jensen, J., Amos, L. A., Gerdes, K., and Lowe, J. (2002) F-actin-like filaments formed by plasmid segregation protein ParM, *EMBO J. 21*, 6935−6943.
40. Osipiuk, J., Walsh, M. A., Freeman, B. C., Morimoto, R. I., and Joachimiak, A. (1999) Structure of a new crystal form of human Hsp70 ATPase domain, *Acta Crystallogr., Sect. D: Biol. Crystallogr. 55*, 1105−1107.
41. Wilbanks, S. M., and McKay, D. B. (1995) How potassium affects the activity of the molecular chaperone Hsc70. II. Potassium binds specifically in the ATPase active site, *J. Biol. Chem. 270*, 2251−2257.
42. Locher, K. P., Hans, M., Yeh, A. P., Schmid, B., Buckel, W., and Rees, D. C. (2001) Crystal structure of the *Acidaminococcus fermentans* 2-hydroxyglutaryl-CoA dehydratase component A, *J. Mol. Biol. 307*, 297−308.
43. Buss, K. A., Cooper, D. R., Ingram-Smith, C., Ferry, J. G., Sanders, D. A., and Hasson, M. S. (2001) Urkinase: Structure of acetate kinase, a member of the ASKHA superfamily of phosphotransferases, *J. Bacteriol. 183*, 680−686.
44. Liao, D. I., Reiss, L., Turner, I., and Dotson, G. (2003) Structure of glycerol dehydratase reactivase: A new type of molecular chaperone, *Structure (Cambridge) 11*, 109−119.
45. Mulichak, A. M., Wilson, J. E., Padmanabhan, K., and Garavito, R. M. (1998) The structure of mammalian hexokinase-1, *Nat. Struct. Biol. 5*, 555−560.
46. Aleshin, A. E., Kirby, C., Liu, X., Bourenkov, G. P., Bartunik, H. D., Fromm, H. J., and Honzatko, R. B. (2000) Crystal structures of mutant monomeric hexokinase I reveal multiple ADP binding sites and conformational changes relevant to allosteric regulation, *J. Mol. Biol. 296*, 1001−1015.
47. Rosano, C., Sabini, E., Rizzi, M., Deriu, D., Murshudov, G., Bianchi, M., Serafini, G., Magnani, M., and Bolognesi, M. (1999) Binding of noncatalytic ATP to human hexokinase I highlights the structural components for enzyme-membrane association control, *Struct. Fold. Des. 7*, 1427−1437.
48. Hurley, J. H., Faber, H. R., Worthylake, D., Meadow, N. D., Roseman, S., Pettigrew, D. W., and Remington, S. J. (1993) Structure of the regulatory complex of *Escherichia coli* IIIGlc with glycerol kinase, *Science 259*, 673−677.
49. Bork, P., Sander, C., and Valencia, A. (1992) An ATPase domain common to prokaryotic cell cycle proteins, sugar kinases, actin, and hsp70 heat shock proteins, *Proc. Natl. Acad. Sci. U.S.A. 89*, 7290−7294.
50. Lu, G. (2000) TOP: A new method for protein structure comparisons and similarity searches, *J. Appl. Crystallogr. 33*, 176−183.
51. Nishino, T., Gallant, J., Shalit, P., Palmer, L., and Wehr, T. (1979) Regulatory nucleotides involved in the Rel function of *Bacillus subtilis*, *J. Bacteriol. 140*, 671−679.
52. Leipe, D. D., Wolf, Y. I., Koonin, E. V., and Aravind, L. (2002) Classification and evolution of P-loop GTPases and related ATPases, *J. Mol. Biol. 317*, 41−72.
53. Akiyama, M., Crooke, E., and Kornberg, A. (1993) An exopolyphosphatase of *Escherichia coli*. The enzyme and its ppx gene in a polyphosphate operon, *J. Biol. Chem. 268*, 633−639.
54. Hara, A., and Sy, J. (1983) Guanosine 5′-triphosphate, 3′-diphosphate 5′-phosphohydrolase. Purification and substrate specificity, *J. Biol. Chem. 258*, 1678−1683.
55. McPhalen, C. A., Strynadka, N. C., and James, M. N. (1991) Calcium-binding sites in proteins: A structural perspective, *Adv. Protein Chem. 42*, 77−144.
56. Essen, L. O., Perisic, O., Katan, M., Wu, Y., Roberts, M. F., and Williams, R. L. (1997) Structural mapping of the catalytic mechanism for a mammalian phosphoinositide-specific phospholipase C, *Biochemistry 36*, 1704−1718.
57. Kraft, L., Sprenger, G. A., and Lindqvist, Y. (2002) Conformational changes during the catalytic cycle of gluconate kinase as revealed by X-ray crystallography, *J. Mol. Biol. 318*, 1057−1069.
58. Harris, T. K., Wu, G., Massiah, M. A., and Mildvan, A. S. (2000) Mutational, kinetic, and NMR studies of the roles of conserved glutamate residues and of lysine-39 in the mechanism of the MutT pyrophosphohydrolase, *Biochemistry 39*, 1655−1674.
59. Zhu, G., Liu, J., Terzyan, S., Zhai, P., Li, G., and Zhang, X. C. (2003) High resolution crystal structures of human Rab5a and five mutants with substitutions in the catalytically important phosphate-binding loop, *J. Biol. Chem. 278*, 2452−2460.
60. Schuler, H., Korenbaum, E., Schutt, C. E., Lindberg, U., and Karlsson, R. (1999) Mutational analysis of Ser14 and Asp157 in the nucleotide-binding site of beta-actin, *Eur. J. Biochem. 265*, 210−220.
61. Yao, X., Grade, S., Wriggers, W., and Rubenstein, P. A. (1999) His(73), often methylated, is an important structural determinant for actin. A mutagenic analysis of HIS(73) of yeast actin, *J. Biol. Chem. 274*, 37443−37449.
62. Kazantsev, A. V., Krivenko, A. A., Harrington, D. J., Carter, R. J., Holbrook, S. R., Adams, P. D., and Pace, N. R. (2003) High-resolution structure of RNase P protein from Thermotoga maritima, *Proc. Natl. Acad. Sci. U.S.A. 100*, 7497−7502.
63. Murzin, A. G. (1995) A ribosomal protein module in EF-G and DNA gyrase, *Nat. Struct. Biol. 2*, 25−26.
64. Laskowski, R. A., MacArthur, M. W., Moss, D. S., and Thornton, J. M. (1993) PROCHECK: A program to check the stereochemical quality of protein structures, *J. Appl. Cryst. 26*, 283−291.
65. Hayward, S., and Berendsen, H. J. (1998) Systematic analysis of domain motions in proteins from conformational change: New results on citrate synthase and T4 lysozyme, *Proteins 30*, 144−154.
66. Thompson, J. D., Higgins, D. G., and Gibson, T. J. (1994) CLUSTAL W: Improving the sensitivity of progressive multiple sequence alignment through sequence weighting, position-specific gap penalties and weight matrix choice, *Nucleic Acids Res. 22*, 4673−4680.

BI049083C